ADVECTION AND DEPOSITION OF MICRODROPLETS IN STAGNATION POINT FLOW

Md Shamser Ali Javed & Vladimir S. Ajaev*

Department of Mathematics, Clements Hall, Southern Methodist University, Dallas, TX, 75275, USA

*Address all correspondence to: Vladimir S. Ajaev, Department of Mathematics, Clements Hall, Southern Methodist University, Dallas, TX, 75275, USA; Tel.: (214) 768-3629; Fax: (214) 768-2355, E-mail: ajaev@smu.edu

Original Manuscript Submitted: 10/22/2023; Final Draft Received: 10/30/2023

We investigate trajectories of microscale evaporating droplets in a stagnation point flow near a wall of a respiratory airway. The configuration is motivated by the problem of advection and deposition of microscale droplets of respiratory fluids in human airways during transmission of infectious diseases, such as tuberculosis and COVID-19. Laminar boundary layer equations are solved to describe the airflow while the equations of motion of the droplet include contributions from gravity, aerodynamic drag, and Saffman force. Evaporation is accounted for at both the droplet surface and the wall of the respiratory airway and is shown to delay droplet deposition as compared to the predictions of isothermal models. Evaporation at the airway wall has a stronger effect on droplet trajectories than evaporation at the droplet surface, leading to droplets being advected away by the flow and thus avoiding deposition in the stagnation point flow region.

KEY WORDS: boundary layer, evaporation, drag force, Saffman force

1. INTRODUCTION

Investigations motivated by environmental or occupational respiratory health requirements strive to comprehend the intricate processes of inhalation and transport of pollutant particles in the human respiratory system. Similar issues arise in the studies of transmission of infectious diseases, such as tuberculosis and COVID-19, by respiratory droplets. The understanding of the motion of particles or droplets through the air and their interactions with the mouth, throat, and upper airways has improved as a result of studies on micro- and nanoparticle transport and deposition over the past several decades. A simplified symmetric anatomical model has been used to predict airflow and particle deposition in many early numerical studies. The development of realistic three-dimensional anatomical models resulted from recent advancements in medical imaging. For example, high-resolution computerized tomography (CT) data provide the accurate portrayal of the respiratory system geometry. The human respiratory system consists of the extrathoracic region, which includes nasal and oral airways, the tracheobronchial region, and the alveolar region. Due to the treelike structure of the tracheobronchial and alveolar regions, they are subdivided in several "generations", labeled by the letter, G. The O₂–CO₂ gas exchange occurs only in the lower part of the system, called the "respiratory zone", corresponding to generations from G17 to G23, while the previous generations form what is referred to as the conducting zone (Silverthorn et al., 2004).

Pioneering numerical flow and particle deposition studies based on biologically relevant geometric configurations were conducted by Yu et al. (1996) and Comer et al. (2001), followed by many others, as reviewed in Kleinstreuer and Zhang (2010). More recent elaborate computational studies were conducted by Feng et al. (2016). Different flow regimes (i.e., laminar, transitional, and turbulent flows) may occur in the airflow in the various airway segments. For example, the flow might be laminar in the oral cavity and transitional or turbulent after the constriction created by the

	NOMENO	CLATURE	
d	droplet diameter, m	η	similarity variable
${f F}$	force	γ	kinematic viscosity, m ² /s
g	acceleration of gravity, m ² /s	ρ	density, kg/m ³
L	air flow length scale, m	ω	vorticity
m Re	mass, kg Reynolds number	Superscript	
St	Stokes number	*	dimensional
u, v	time velocity components	Subsc	Subscripts
x, y	Cartesian coordinates	d	droplet
-		D	drag
Greek Symbols		0	initial
α	flow parameter	s	shear
u	dynamic viscosity, Pa s	S	Stefan or Saffman

soft palate and throat, but it might eventually become laminar flow again after several generations in the bronchial, tree because the local Reynolds number gradually decreases.

Once the flow structure is determined, conclusions can be made about the deposition of nano- and microscale particles and droplets. Studies of deposition of particles or droplets on solid surfaces have a long history and were conducted in the context of several different applications (Wong et al., 1955; Noll and Pilat, 1970; Fichman et al., 1990; Issa and Yao, 2005). For situations when inertia and gravity effects are negligible, small particles are expected to follow the flow streamlines and avoid deposition on the solid surface. However, in practice the effects of inertia are typically not negligible, even for very small particles and droplets. As a result, when flow streamlines change direction, the particles are unable to follow them and continue to move along nearly straight paths as a result of particle inertia, leading to possible deposition on the solid surface. This phenomenon is usually called inertial impaction or simply impaction. Also, gravity can play a role, leading to gravitational sedimentation. Nonuniformity of fluid velocity around the droplet or particle leads to a so-called Saffman lift force (Saffman, 1965; Mei, 1992). For nanoscale particles, the effects of Brownian diffusion are relevant. Several additional effects have to be taken into account when the unsteady nature of the flow is considered; these are beyond the scope of the present article.

For applications to the respiratory system, it has been well established that droplet deposition patterns strongly depend on the droplet size, as illustrated in Fig. 1. Here, the deposition enhancement factor (DEF) is the key measure of nonuniformity of deposition patterns, defined as the ratio of local deposition density to the average value of the same quantity. The values of DEF can be as high as 10^3 for microdroplets, but are typically between 1 and 10 for nanoparticles.

In the present study, we focus on microscale droplets. Impaction and secondary flow convection can play a role in microparticle deposition in large airways during inhalation, such as the nasal, oral, and upper tracheobronchial airways. As a result, most of these particles accumulate near stagnation spots. The carinal ridges are the principal locations for micron–particle depositions in big bronchial airways (see Fig. 1). Gravitational sedimentation cannot be ignored in medium- to small-sized airways, leading to shifts in the deposition patterns and causing the DEF values to drop. In particular, Zhang et al. (2009) showed that, due to gravitational settling, the maximum DEF values may decrease by an order of magnitude for micron-sized particles.

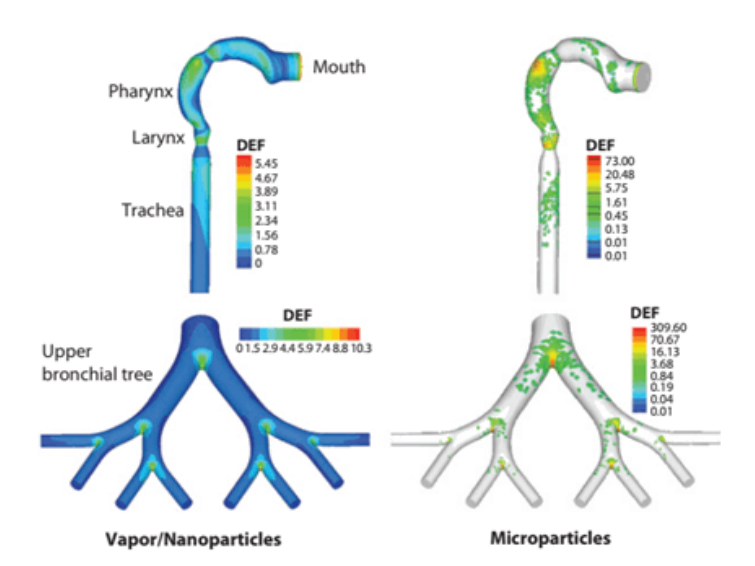


FIG. 1: Deposition enhancement factors for an upper airway model, reprinted from Zhang et al. (2005), with permission from Elsevier, Copyright 2005

A closely related area of research is on particle dispersions. The concentration and inertia of the particles affect the flow in two-phase boundary layers (Varaksin, 2020). The inertia of particles as they move in the boundary layer should be taken into consideration. It depends on the flow geometry and characteristics and might change for the same particles. The analysis of these flows and the generalization of the data are made more difficult by the existence of various characteristic times and lengths of the flow. Due to particle deceleration in the vicinity of the wall, particle interaction with the wall, and particle collisions, the profile of particle concentration in a boundary layer can have a complex pattern. The primary objectives in the investigation of two-phase boundary layers in dispersions are to investigate particle motion in the boundary layer and to identify the feedback effect of particles on fluid properties. In the present article, we assume the droplet concentration in the airflow to be sufficiently low and thus the modifications of the flow due to presence of particles are not considered.

Our key objectives are to study how trajectories of microscale droplets in a region near a stagnation point on the airway wall depend on flow properties, droplet sizes, and the evaporation rates at the droplet surface and airway wall. The consideration of phase change at the airway wall represents the key novelty of the research described in the present study.

2. LOCAL FLOW STRUCTURE

The global airflow structure can only be obtained from detailed numerical solutions of the Navier–Stokes equations, as discussed in the Introduction. However, since the focus of the present work is on interactions of droplets with airways, leading to their deposition on the walls, we can get a number of useful insights into the physics of the process by using local flow solutions. Specifically, we apply the stagnation flow model at an airway bifurcation, as illustrated in Fig. 2. The objective of this section is to summarize the relevant results on the stagnation point boundary layer structure needed to describe the motion of droplet. The flow velocity components outside of the boundary layer are given by

$$u^* = \alpha x^*, \qquad v^* = -\alpha y^*, \tag{1}$$

where α is a positive dimensional constant, x^* and y^* are local Cartesian coordinates in the two-dimensional approximation used. Let us scale the velocity components by the characteristic external flow speed U, the length variables by $L = U/\alpha$, and define the Reynolds number, $Re = UL/\nu$, where ν is the kinematic viscosity of air. Note that L can be interpreted as the size of the region in which the stagnation point flow model is applicable and is typically

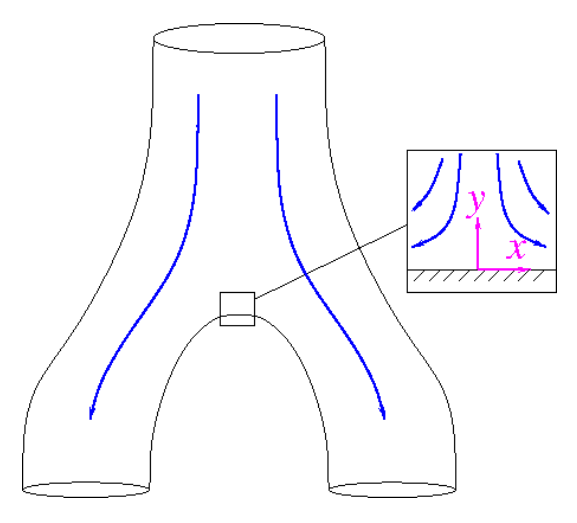


FIG. 2: Sketch of the geometric configuration that motivates the analysis of the stagnation point flow

much smaller than global flow length scales, such as the diameter of the airway. The typical range of values of Re of interest for the present study is 1–100, so the flow can be assumed laminar. Furthermore, the time between droplet entering the stagnation point flow domain and its deposition or removal by the flow is assumed to be much shorter than the time length of the breathing cycle. The stagnation point flow stream function has a self-similar form, with the nondimensional velocity components expressed as follows:

$$u = xf'(\eta), \qquad v = -Re^{-1/2}f(\eta),$$
 (2)

where $\eta = \text{Re}^{1/2}y$ is the similarity variable. Substitution of the expressions in Eq. (2) for velocity components into Prandtl boundary layer equations leads to an ordinary differential equation for $f(\eta)$,

$$f''' + ff'' + 1 - f'^2 = 0. (3)$$

The no-slip condition at the airway wall and the matching condition to the inviscid flow pattern outside the boundary layer are expressed as follows:

$$f'(0) = 0, f'(\infty) = 1.$$
 (4)

The standard no-penetration condition has to be modified to account for the fact that evaporation is possible from the airway wall, which is covered by aqueous mucus. Evaporation induces flow in air of scaled velocity v_S in the normal direction to the wall, known as Stefan flow (Sazhin, 2014), leading to the nondimensional boundary condition

$$f(0) = -Re^{1/2}v_S. (5)$$

This condition completes the formulation. While originally derived in the context of the boundary layer theory, the viscous stagnation point flow, also called Hiemenz flow, turns out to be an exact solution of the Navier–Stokes equations. Equation (3), with the conditions (4) and (5), has been solved numerically using the bvp4c subroutine in Matlab. A typical streamline pattern is shown in Fig. 3. Note that evaporation-induced flow acts against the external flow directed toward the wall.

3. MODEL OF DROPLET MOTION

The integration of the droplet equations of motion in the airflow described in Section 2, is used to compute the droplet trajectories and determine the location of deposition on the wall of the airway.

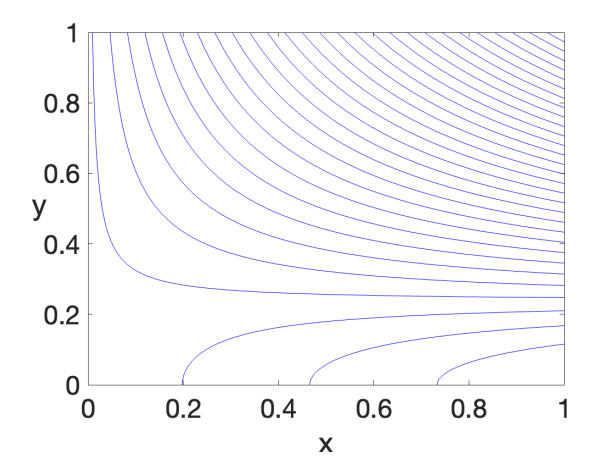


FIG. 3: Structure of the viscous stagnation point flow near the airway wall in the presence of evaporation, with Re = 20, $v_S = 0.1$. Half of the symmetric flow pattern is shown.

3.1 Dimensional Formulation

We consider a spherical liquid droplet of density ρ_d and diameter d. The latter can be fixed or time-dependent as a result of phase change, such as evaporation or condensation. While a number of droplets can be present in the flow, we expect their concentration to be not high enough to affect the flow structure or to make the droplet—droplet interactions an important factor. In the formulation [Eqs. (6) and (7)], we also neglect the effects of buoyancy and Magnus force. With these assumptions, the equations of droplet motion take the following form:

$$\frac{d\mathbf{x}_d^*}{dt^*} = \mathbf{u}_d^*,\tag{6}$$

$$m_d \frac{d\mathbf{u}_d^*}{dt^*} = \mathbf{F}_D^* + \mathbf{F}_S^* + m_d \mathbf{g},\tag{7}$$

where \mathbf{x}_d^* is the droplet radius vector; \mathbf{u}_d^* is the instantaneous droplet velocity, m_d is the droplet mass ($m_d = \pi \rho_d d^3/6$, ρ_d being liquid density); \mathbf{F}_D^* is the aerodynamic drag force, \mathbf{F}_S^* is the Saffman force, which is essentially the lift force, which arises due to airflow velocity gradient near the droplet, as discussed in more detail below, and \mathbf{g} is the acceleration of gravity. Both the lift force and gravity term are smaller in magnitude than the drag force in typical simulations described in Section 4.

3.2 Drag Force

The drag force, represented by the term \mathbf{F}_D^* in Eq. (7), arises due to the difference between the airflow velocity and the velocity of a droplet moving through the air, and can be written in dimensional form as follows:

$$\mathbf{F}_D^* = C_D \frac{\rho \pi d^2}{8} \left| \mathbf{u}^* - \mathbf{u}_d^* \right| (\mathbf{u}^* - \mathbf{u}_d^*), \tag{8}$$

where C_D is the aerodynamic drag coefficient which is a function of the Reynolds number based on the droplet size, $\operatorname{Re}_d = |\mathbf{u}^* - \mathbf{u}_d^*| \, d/\nu$. In the limiting case of $\operatorname{Re}_d = 0$, the drag force can be calculated based on the Stokes flow equations, leading to $C_D = 24/\operatorname{Re}_d$, as was done in several recent studies of microdroplet trajectories (Kabov et al., 2016, 2017; Ajaev and Kabov, 2021). A number of corrections to the classical Stokes result have been introduced for nonzero droplet Reynolds numbers, starting with the Oseen formula. A commonly used approximation that describes a wider range of Reynolds numbers (Clift et al., 2005; Varaksin, 2020) is given by:

$$C_D = \frac{24}{\text{Re}_d} \left(1 + \frac{1}{6} \text{Re}_d^{2/3} \right). \tag{9}$$

3.3 Saffman Force

Let us now discuss the effect of the airflow velocity profile nonuniformity on the droplet motion (Saffman, 1965). A pressure difference emerges as a result of the spatial variation in relative velocities of the flow past a droplet. As the pressure decreases locally, the droplet will migrate in the direction of lower pressure, a phenomenon that is often interpreted as action of lift force called the Saffman force. The expression for the dimensional Saffman force has the form (Mei, 1992)

$$\mathbf{F}_S^* = C_S \frac{\rho \pi d^3}{16} \{ (\mathbf{u}^* - \mathbf{u}_d^*) \times \mathbf{\omega}^* \},\tag{10}$$

where $\mathbf{w}^* = (\nabla \times \mathbf{u}^*)$ is the vorticity of the airflow. Here, the original result of Saffman (1965) is modified by the correction function C_S , as follows:

$$C_S = \frac{4.1126}{\text{Re}_a^{0.5}} C(\text{Re}_d, \text{Re}_s), \tag{11}$$

where the Reynolds number based on the local the shear flow is $Re_s = |\mathbf{w}^*| d^2/(2\nu)$ and the new function $C(Re_d, Re_s)$ is defined, following Varaksin (2020), as follows:

$$C = \begin{cases} (1 - 0.3314\beta^{1/2})\exp(-\text{Re}_d/10) + 0.3314\beta^{1/2}, & \text{Re}_d \le 40\\ 0.0524\beta^{1/2}\text{Re}_d^{1/2}, & \text{Re}_d > 40 \end{cases}$$
 (12)

Here, we introduce a new parameter β

$$\beta = \frac{|\mathbf{w}^*| d}{4 |\mathbf{u}^* - \mathbf{u}_d^*|} = \frac{1}{2} \frac{\text{Re}_s}{\text{Re}_d}.$$
 (13)

Finally, we observe that due to the two-dimensional nature of the flow,

$$\mathbf{w}^* = \left(\frac{\partial v^*}{\partial x^*} - \frac{\partial u^*}{\partial y^*}\right) \mathbf{k},\tag{14}$$

where k is the unit vector in the direction of the z-axis.

3.4 Nondimensionalization

Let us now scale the droplet velocity by U, the characteristic air flow velocity, and time by L/U, leading to the nondimensional version of Eq. (6),

$$\frac{d\mathbf{x}}{dt} = \mathbf{u}_d. \tag{15}$$

In order to complete the nondimensional formulation of the equations of motion for the droplet, we now proceed to rewriting the expressions for forces discussed in Sections 3.2 and 3.3 in terms of the scaled velocity components. The drag force can be written as follows:

$$\mathbf{F}_D^* = 3\pi\mu U d\hat{C}_D(\mathbf{u} - \mathbf{u}_d),\tag{16}$$

where $\hat{C}_D=1+\mathrm{Re}_d^{2/3}/6.$ The dimensional Saffman force can be expressed as

$$\mathbf{F}_{S}^{*} = C_{S} \frac{\rho \pi d^{3} U^{2}}{16L} \mathbf{f}, \qquad \mathbf{f} = \left(\frac{\partial v}{\partial x} - \frac{\partial u}{\partial y}\right) \left[\mathbf{i}(v - v_{d}) - \mathbf{j}(u - u_{d})\right]. \tag{17}$$

This result together with Eq. (16) for the drag force leads to a nondimensional version of Eq. (7) written in terms of the Stokes number, St. as follows:

$$\frac{d\mathbf{u}_d}{dt} = \frac{\hat{C}_D}{\mathrm{St}}(\mathbf{u} - \mathbf{u}_d) + \frac{3\hat{\rho}C_S}{8}\mathbf{f} + \hat{\mathbf{g}}, \quad \mathrm{St} = \frac{\rho_d d^2 U}{18\mu L}.$$
 (18)

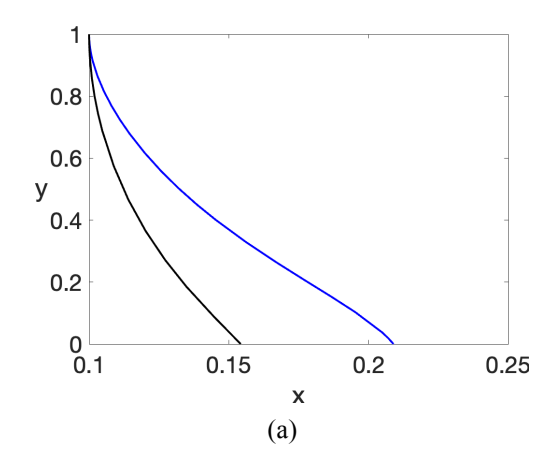
where $\hat{\rho}$ is the air-to-liquid density ratio and \hat{g} is the acceleration of gravity scaled by U^2/L . While the latter can be expressed in terms of the inverse Froude number, we find it more convenient to use the magnitude of \hat{g} , denoted by \hat{g} . Nondimensional equations (15) and (18) represent the complete nondimensional formulation for studies of droplet trajectories. We solved these equations numerically using the ode15s subroutine from Matlab with the airflow field \mathbf{u} found in Section 2.

4. RESULTS AND DISCUSSION

Let us start by investigating local droplet trajectories in the limit when phase change at both the airway wall and droplet surface is negligible. The key nondimensional parameters are then the Reynolds numbers, Stokes number, and density ratio $\hat{\rho}$. Let us start by considering a droplet of fixed size and density under different flow conditions characterized by the Reynolds numbers and Stokes number, corresponding to different locations in the respiratory system. Here and below we choose the initial droplet location in the domain, (0.1,1), close to the axis of symmetry; although, the key conclusions are the same for a number of different initial locations. We evaluate the nondimensional parameters based on the droplet size of $10~\mu m$. For a small Reynolds number, the Stokes drag law is applicable and the droplet tends to be essentially carried by the flow. The same tendency can be observed for a range of Reynolds numbers close to and >1. However, as Re is increased further, droplet deposition is observed [illustrated at Re = 5 by the right line in Fig. 4(left)], and it tends to take place closer to the axis of symmetry for larger flow Reynolds numbers, as also seen in the plot. We adjust the value of the Stokes number to describe a situation in which the characteristic dimensional airflow speed is the only parameter being varied. The droplet and shear Reynolds numbers, as well as \hat{g} , are recalculated based on U corresponding to the specified flow Reynolds number, using $v = 1.66 \times 10^{-5}~\text{m}^2/\text{s}$ and $L = 10^{-3}~\text{m}$.

For a fixed location in the respiratory system, the droplets of different sizes can have different trajectories. Let us consider a typical value of the flow Reynolds number, Re=10. We find that in the range of droplet sizes between 10 and 30 μ m, even relatively small changes in the droplet size can change the location of deposition, as illustrated in Fig. 4(right). Larger droplets of size >50 μ m travel through the boundary layer region in a nearly straight line. Our model also suggests that only droplets of size of ~ 1 μ m or smaller can avoid being deposited, but it is important to keep in mind that the model is likely to break down for such small droplets.

Let us now consider the effect of phase change on advection and deposition of droplets. Under the conditions of moderate humidity and physiologically relevant temperatures, small droplets are likely to decrease their size by



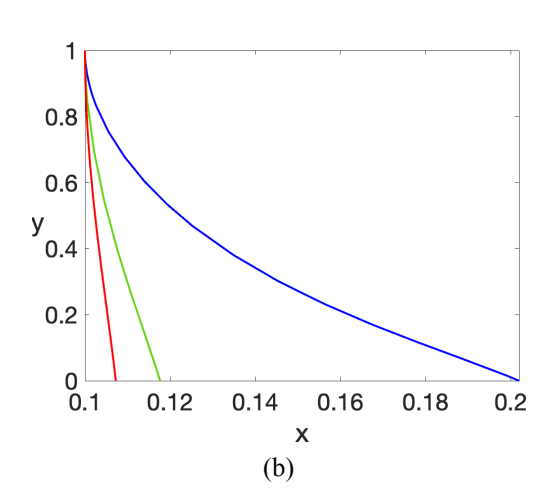


FIG. 4: Typical droplet trajectories in nondimensional coordinates plotted for different values of the flow Reynolds number, Re = 20, St = 1 (left line), Re = 5, St = 0.25 (right) (plot on the left), and different droplet sizes at Re = 10: $d = 10 \mu m$ (right), $d = 20 \mu m$ (middle line), $d = 30 \mu m$ (far left line)(plot on the right)

evaporation. The dynamics of this process is very well established, and it is typically described by the so-called d^2 -law, which can be incorporated into our nondimensional formulation by using

$$\hat{d} = \hat{d}_0 \left(1 - \gamma t \right)^{1/2},\tag{19}$$

where the nondimensional parameter γ characterizes the evaporation rate, which depends on temperature and humidity.

Since evaporation reduces droplet size and we already established that smaller droplets travel further before getting deposited, as seen in Fig. 4(right), it is natural to expect that evaporation will delay deposition. This is indeed seen on our simulations for several different values of γ , illustrated in Fig. 5. However, for realistic values of γ , the effect is not very strong. For example, even the largest value seen in Fig. 5 shows a shift of the deposition location coordinate of $\sim 10\%$ in the direction away from the axis of symmetry. No droplets are seen to be leaving the simulation domain, i.e., being advected away by the flow instead of being deposited. Although we are following an individual droplet here, in reality there are typically many droplets present in the flow, so the deposition process should be described in terms of a distribution of deposition locations. Our results for the individual droplets suggest that the distribution is modified due to droplet evaporation, with less deposition at the symmetry line of the local stagnation point flow and more deposition away from it. However, the fraction of droplets, which completely avoid deposition and end up traveling further into the respiratory system, does not change significantly when evaporation from the droplet surface is taken into consideration.

Evaporation can take place not only at the droplet surface but also at the airway walls, which are covered by aqueous mucus. Due to its high viscosity, the no-slip boundary condition for the airflow at the airway wall is still a good approximation, but evaporation from the wall requires modification of the no-penetration condition, as was outlined in Section 2. We investigated droplet trajectories for a range of values of scaled Stefan flow velocity and found that the droplet behavior can be altered dramatically by this previously neglected phenomenon. This is illustrated in Fig. 6. For sufficiently large v_S , the droplet trajectory has a minimum and then moves away from the wall. In physical terms, this can be explained by the action of upward flow generated by evaporation, as is observed in studies of levitation of microdroplets over evaporating liquid layers (Ajaev and Kabov, 2021).

5. CONCLUSIONS

Motion of microscale droplets in stagnation point flow has been investigated and shown to be affected by a number of factors such gravity, aerodynamic drag, and Saffman lift force. For a range of realistic conditions, the drag force is the primary factor determining droplet motion. For models which neglect phase change effects, the key nondimensional

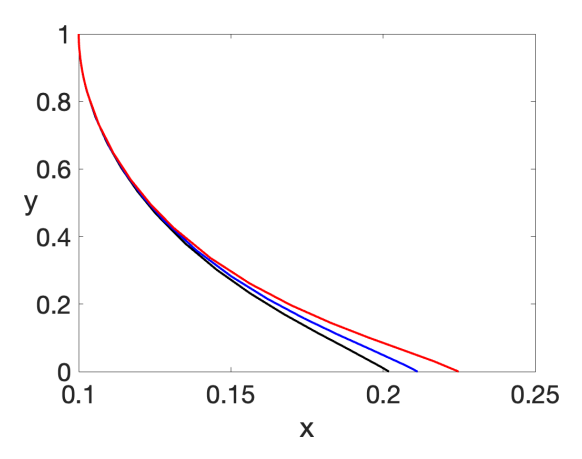


FIG. 5: Trajectories of evaporating droplets in the stagnation point flow at Re = 10, St = 0.5, $v_S = 0$, and different values of droplet evaporation rate, measured by γ : $\gamma = 0$ (left line), $\gamma = 0.1$ (middle line), $\gamma = 0.2$ (right line)

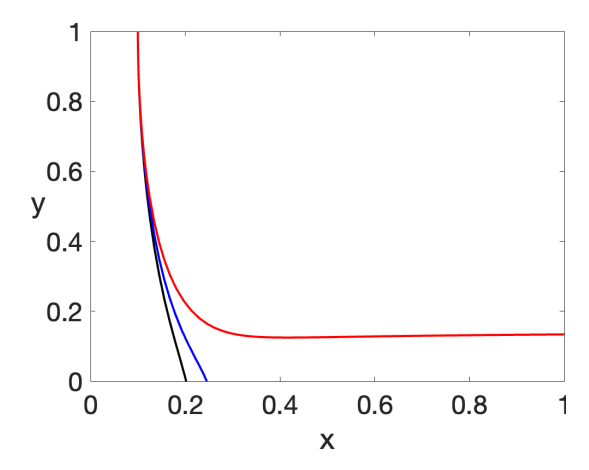


FIG. 6: Illustration of the effect of evaporation from an airway wall on motion of droplets. Trajectories are shown for Re = 10, $\gamma = 0$, and three different values of the Stefan flow velocity: $v_S = 0$ (far left line), $v_S = 0.1$ (middle line), and $v_S = 0.2$ (far right line).

parameters are the flow Reynolds number, the Stokes number, the droplet Reynolds number, the shear Reynolds number, and the density ratio. Increasing the flow Reynolds number leads to deposition closer to the axis of symmetry of the stagnation point flow. Other parameters can be varied by changing the droplet size, which is relevant for the applications as droplets entering the respiratory airways can have a range of sizes. Smaller droplets travel further before being deposited at the airway wall.

Evaporation at the droplet surface reduces the droplet size and thus delays droplet deposition, but for a range of realistic evaporation rates this effect is not particularly strong. However, when evaporation at the airway wall is considered, it leads to significant changes in droplet trajectories. Droplets can be repelled from the airway wall as a result of evaporation and end up being advected away from the wall instead of being deposited there. This phenomenon is not considered in the commonly used models of droplet deposition in respiratory airways.

There are many effects which are of interest for future directions of research, most notably time periodic variations in the air flow structure, droplet rotation, as well as Knudsen layer effects for very small droplets.

ACKNOWLEDGMENT

The work was supported by the U.S. National Science Foundation Grant No. DMS-2009741.

REFERENCES

Ajaev, V.S. and Kabov, O.A., Levitation and Self-Organization of Droplets, *Annu. Rev. Fluid Mech.*, vol. **53**, pp. 203–225, 2021. Clift, R., Grace, J.R., and Weber, M.E., *Bubbles, Drops, and Particles*, Mineola, NY: Dover Publications, 2005.

Comer, J.K., Kleinstreuer, C., and Zhang, Z., Flow Structures and Particle Deposition Patterns in Double-Bifurcation Airway Models. Part 1. Air Flow Fields, *J. Fluid Mech.*, vol. **435**, pp. 25–54, 2001.

Feng, Y., Kleinstreuer, C., Castro, N., and Rostami, A., Computational Transport, Phase Change and Deposition Analysis of Inhaled Multicomponent Droplet–Vapor Mixtures in an Idealized Human Upper Lung Model, *J. Aerosol Sci.*, vol. **96**, pp. 96–123, 2016.

Fichman, M., Pnueli, D., and Gutfinger, C., Aerosol Deposition in the Vicinity of a Stagnation Point, *Aerosol Sci. Technol.*, vol. 13, pp. 281–296, 1990.

Issa, R.J. and Yao, S.C., Numerical Model for Spray-Wall Impaction and Heat Transfer at Atmospheric Conditions, *J. Thermophys. Heat Transf.*, vol. **19**, no. 4, pp. 441–447, 2005.

Kabov, O.A., Zaitsev, D.V., Kirichenko, D.P., and Ajaev, V.S., Investigation of Moist Air Flow near Contact Line Using Microdroplets as Tracers, *Interfac. Phenom. Heat Transf.*, vol. 4, nos. 2-3, pp. 207–216, 2016.

- Kabov, O.A., Zaitsev, D.V., Kirichenko, D.P., and Ajaev, V.S., Interaction of Levitating Microdroplets with Moist Air Flow in the Contact Line Region, *Nanosc. Microsc. Thermophys. Eng.*, vol. **21**, no. 2, pp. 60–69, 2017.
- Kleinstreuer, C. and Zhang, Z., Airflow and Particle Transport in the Human Respiratory System, *Annu. Rev. Fluid Mech.*, vol. **42**, pp. 301–334, 2010.
- Mei, R., An Approximate Expression for the Shear Lift Force on a Spherical Particle at Finite Reynolds Number, *Int. J. Multiphase Flow*, vol. **18**, no. 1, pp. 145–147, 1992.
- Noll, K.E. and Pilat, M.J., Inertial Impaction of Particles upon Rectangular Bodies, *J. Colloid Interf. Sci.*, vol. **33**, no. 2, pp. 197–207, 1970.
- Saffman, P.G., The Lift on a Small Sphere in a Slow Shear Flow, J. Fluid Mech., vol. 22, no. 2, p. 385, 1965.
- Sazhin, S., Droplets and Sprays, New York: Springer, 2014.
- Silverthorn, D.U., Ober, W.C., Garrison, C.W., Silverthorn, A.C., and Johnson, B.R., *Human Physiology: An Integrated Approach*, vol. **3**, Indianapolis, IN, Pearson Education, 2013.
- Varaksin, A.Yu., Two-Phase Boundary Layer of Gas with Solid Particles, High Temp., vol. 58, no. 5, pp. 716–732, 2020.
- Wong, J.B., Ranz, W.E., and Johnstone, H.F., Inertial Impaction of Aerosol Particles on Cylinders, *J. Appl. Phys.*, vol. 26, no. 2, pp. 244–249, 1955.
- Yu, G., Zhang, Z., and Lessmann, R., Computer Simulation of the Flow Field and Particle Deposition by Diffusion in a 3D Human Airway Bifurcation, *Aerosol Sci. Technol.*, vol. **25**, no. 3, pp. 338–352, 1996.
- Zhang, Z., Kleinstreuer, C., Donohue, J.F., and Kim, C.S., Comparison of Micro- and Nano-Size Particle Depositions in a Human Upper Airway Model, *J. Aerosol Sci.*, vol. **36**, no. 2, pp. 211–233, 2005.
- Zhang, Z., Kleinstreuer, C., and Kim, C.S., Comparison of Analytical and CFD Models with Regard to Micron Particle Deposition in a Human 16-Generation Tracheobronchial Airway Model, *J. Aerosol Sci.*, vol. **40**, no. 1, pp. 16–28, 2009.